PCCP

PAPER

View Article Online
View Journal | View Issue

Cite this: *Phys. Chem. Chem. Phys.*, 2017, **19**, 16819

Theoretical study of gas and solvent phase stability and molecular adsorption of noncanonical guanine bases on graphene†

Nabanita Saikia, *[a] Shashi P. Karna[b] and Ravindra Pandey*[a]

The gas and solvent phase stability of noncanonical $(Gua)_n$ nucleobases is investigated in the framework of dispersion-corrected density functional theory (DFT). The calculated results strongly support the high tendency for the dimerization of $(Gua)_n$ bases in both gas and solvent phases. An interplay between intermolecular and bifurcated H-bonds is suggested to govern the stability of $(Gua)_n$ bases which bears a correlation with the description of dispersion correction terms employed in the DFT calculations. For example, a higher polarity is predicted for $(Gua)_n$ bases by the dispersion-corrected DFT in contrast to the non-polar nature of $(Gua)_3$ and $(Gua)_4$ predicted by the hybrid meta-GGA calculations. This distinct variation becomes significant under physiological conditions as polar $(Gua)_n$ is likely to exhibit greater stabilization in the gas phase compared to solvated $(Gua)_n$. Graphene acting as a substrate induces modification in base configurations *via* maximization of π-orbital overlap between the base and substrate. In solvent, the substrate-induced effects are further heightened with lowering of the dipole moments of $(Gua)_n$ as also displayed by the corresponding isosurface of the electrostatic potential. The graphene-induced stability in both gas and solvent phases appears to fulfill one of the prerequisite criteria for molecular self-assembly. The DFT results therefore provide atomistic insights into the stability and molecular assembly of free-standing noncanonical $(Gua)_n$ nucleobases which can be extended to understanding the self-assembly process of functional biomolecules on 2D materials for potential biosensing applications.

Received 4th May 2017,
Accepted 2nd June 2017

DOI: 10.1039/c7cp02944f

rsc.li/pccp

I. Introduction

Deoxyribonucleic acid (DNA) is one of the fundamental building blocks of life that decodes the genetic information, guides protein synthesis and finds potential applications as biosensors in nanoelectronic devices.[1] The four nucleobases, *viz.* adenine (Ade), guanine (Gua), cytosine (Cyt) and thymine (Thy), determine the functionality and fascinating chemistry of DNA like self-recognition and molecular assembly. In particular, Gua ($C_5H_5N_5O$), a nitrogenous nucleobase comprising of a fused pyrimidine-imidazole ring, has drawn significant research interest over the past few years. There exists three H-bond acceptor (N_7, N_3, and O_6) and two H-bond donor (N_1, and N_2) sites (Fig. 1, left panel) which subsequently act as Brønsted acid and base (pK_a = 3.3, 9.2, and 12.3 *vs.* 4.45 and 12.2 for carbon), respectively.[2] An isosurface plot of the electrostatic potential (ESP) (Fig. 1, right panel) displays regions of high (negative) electron density residing

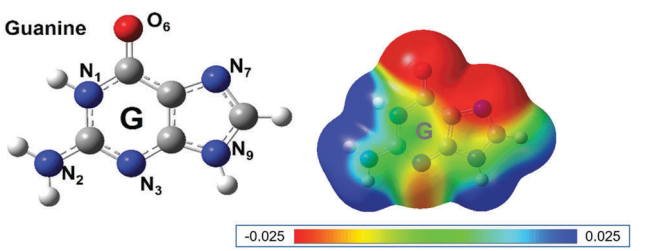

Fig. 1 Guanine: (left) schematic of the H-bond donor (N_1, N_2) and acceptor (N_7, N_3, O_6) sites, (right) isosurface plot of the electrostatic potential (ESP) in the gas phase.

[a] *Department of Physics, Michigan Technological University, Houghton, Michigan, USA. E-mail: nsaikia@mtu.edu, pandey@mtu.edu; Tel: +1-906-487-2086*
[b] *Weapons and Materials Research Directorate, U.S. Army Research Laboratory, ATTN: RDRL-WM, Aberdeen Proving Ground, Aberdeen, Maryland 21005-5069, USA*

† Electronic supplementary information (ESI) available: The equilibrium configurations of $(Gua)_n$ complexes in the solvent phase at the wB97XD and M05-2X levels of theory. The relative stability and dipole moment values of $(Gua)_n$ bases in the solvent phase. The ESP isosurface of $(Gua)_n$ in gas and solvent phases at the PBE-D2 and M06-2X levels. The equilibrium configuration and ESP isosurface of Gua/graphene in gas and solvent phases, interaction energy, dipole moment and average H-bond distance for Gua and $(Gua)_2$ complexes treated with the implicit solvation model, and Gua/graphene calculated at the PBE-D2 level. The stacked configurations along with the ESP isosurface for $(Gua)_2$/graphene and $(Gua)_4$/graphene in gas and solvent phases. See DOI: 10.1039/c7cp02944f

on O_6, N_7, and N_3 atoms corresponding to electron accepting moieties and N_1 and N_2 as regions with low electron density or electron donating moieties. What makes Gua relevant is its low ionization potential (7.77–7.85 eV) and strong electron-donor characteristics (E_{ox} = +1.25 V *vs.* Saturated Calomel Electrode (SCE)),[3] which facilitates charge transport in Gua-based molecular complexes.[4,5]

Apart from the conventional Watson–Crick canonical base pairs, noncanonical base pairs constitute about 40% of the nucleobase pairs in triplets and tertiary interactions and are of potential biological relevance.[6,7] For example, Gua-rich moieties are abundant in the human genome with a high propensity to fold into hierarchical structural motifs facilitated by hydrophobic interactions.[8,9] They can form an array of self-assembled nanostructures like the $(Gua)_4$ quadruplex,[10] where the Gua base pairs fold through Hoogsteen H-bonds. The G-rich moieties can exhibit an exquisite internal H-bonded motif,[11,12] *e.g.* honeycomb arrangements,[13] nanowires[14] and sheet-like assemblies.[15,16] Dimerization within analogous nucleobases is an inherent characteristic facilitated by the polar, electronegative oxygen and nitrogen heteroatoms. In Gua, the presence of donor/acceptor sites determines its propensity to oligomerize which are mediated by the noncovalent H-bonds.[17] For example, the Gua-quartet is found to exhibit three types of H-bonding patterns; Hoogsteen-type, two bifurcated and four bifurcated bonds. The complexes with four bifurcated H-bonds demonstrate the highest stability whereas lack of bifurcated H-bonds results in energetically least-stable structures.[18] Furthermore, it was suggested that incorporation of a cation in the Gua-quartet leads to Hoogsteen-type H-bond patterns.[19]

In general, the supramolecular self-assembly of biological/functional molecules is mitigated in the presence of an inorganic solid substrate which serves as the template for growth and fabrication.[20] In most cases, an array of diverse geometries (polymorphs) is observed and the efficacy of the substrate on monolayer assembly dictates the molecular orientation and adsorption.[21–23] For example, imaging the self-assembly of Gua molecules on freshly cleaved highly ordered pyrolytic graphite (HOPG),[24] *via* MAC mode Atomic Force Microscopy showed that Gua molecules condense (aggregate) in small nuclei or clusters (20–40 nm in diameter and 2–3 nm in height) with uniform coverage on HOPG, without any well-ordered array. The change in exposure time from 5 min to 1 hour led to the reorganization of Gua clusters. Furthermore, experimental studies on the molecular packing of Ade nucleobases on the graphite (0001) surface reported that Ade molecules are stabilized by an intermolecular H-bonded network with four H-bonds per Ade molecule along the graphite surface.[25]

Graphene has generally served as an ideal 2D candidate for fabrication of novel bio-integrated structures[26] due to its atomically flat surface together with unique physical, optical and electronic properties. Given the complexity of simulating the interface of a bio-integrated material at an atomistic level, a detailed understanding of a crossover mechanism in base–base and base–substrate interactions therefore becomes a prerequisite condition for technological applications of bio-integrated materials at the nanoscale.

It is well known that a reliable description of noncovalently bonded systems[27] requires specific terms representing dispersion interactions in the electronic structure calculations. In general, the dispersion forces, which arise from the correlated motion of electrons,[28] comprise the dominant '*long-range*' effect.[29–32] For Gua-complexes, previous density functional theory (DFT) studies employed either the hybrid B3LYP/6-311G(d,p)[19] or the hybrid meta-GGA M06-2X/6-31+G(d,p) level of theory.[33] The hybrid meta-GGA functional form implicitly accounts for the '*medium-range*' ($\sim$2–5 Å) electron correlation, and falls off exponentially at the '*long range*' ($\sim$5 Å) thereby lacking the nonlocality to support the R^{-6} asymptotic distance-dependence decay.[34] Grimme's empirical dispersion correction (D2) uses an empirically derived interpolation formula[35,36] by taking into account the long-range correlation interactions.[37] Here, the C_6 coefficient captures most of the correct asymptotic behavior in the long-range, with its role diminishing at short distances.[38]

Considering noncanonical $(Gua)_n$ bases as an example, the present study aims at providing an atomistic-level understanding of the role played by (i) the choice of dispersion interaction terms in DFT calculations, (ii) the usefulness of the implicit *vs.* the explicit solvent model and (iii) the role of graphene as a substrate in assimilating the monolayer adsorption and self-assembly of guanine bases. Realizing that our choice of the substrate represents a weakly interacting (physisorbed) surface, the objective will then be to quantify the substrate-induced effects on the energetics and electronic properties of $(Gua)_n$ bases. To address the question of how the stability of $(Gua)_n$ bases depends on the choice of the dispersion term, Grimme's correction term together with the hybrid meta-GGA M06-2X functional form[39] is considered. Since the molecular interactions under physiological conditions are expected to be different from those in the gas phase, solvent phase calculations are performed. We believe that an understanding of the ability to regulate oligomerization of noncanonical $(Gua)_n$ bases with and without the substrate can help establish a systematic approach towards integrating 2D materials for supramolecular self-assembly at the nanoscale.

II. Computational model

The stability and electronic properties of $(Gua)_n$ bases with n = 2–6 in gas and solvent phases were investigated in the framework of dispersion-corrected DFT. The exchange correlation potential was described by the Generalized Gradient Approximation (GGA) using the Perdew–Burke–Ernzerhof (PBE) functional[40] and a 6-31G(d,p) basis set.[41] Since the PBE functional has shortcomings in terms of the accurate description of the self-interaction error and noncovalent vdW interactions,[42,43] Grimme's empirical correction (D2) term was included. Although Grimme's D2 method is not the sole benchmark model for accounting the noncovalent van der Waals (vdW) interactions, it provides comparable results at a reasonable computational cost compared to computationally expensive methods like CCSD(T).[44,45] For consistency with our prior reports,[46,47] we considered the

6-31G(d,p) basis set with the PBE-D2 functional. Additional calculations were carried out using the dispersion corrected wB97XD, M05-2X and M06-2X functionals to supplement previous DFT studies on the structure and stability of free-standing $(Gua)_n$ complexes.[34] Note that the 6-31+G(d,p) basis set implemented with the M06-2X functional includes one set of sp-type diffuse functions to the non-H atoms yielding slightly lower total energy values compared to a 6-31G(d,p) basis set. All the calculations were performed using Gaussian09,[48] with the maximum force convergence for geometry optimization set to 10^{-4} eV Å^{-1}. The convergence criteria in the density matrix and the total energy were 10^{-8} and 10^{-6} eV, respectively.

To simulate the solvent effects, we employed the implicit solvent model in which the polar solute interacts with the surrounding dielectric medium through dipolar interactions. The solvent medium was represented by the polarizable continuum model (PCM)[49] with a dielectric constant of 78.36 for water. In principle, a comprehensive comparison of implicit *vs.* explicit solvents serves as an effective route to mimic the influence of waters towards the intermolecular interactions and molecular stability. However, we considered the implicit solvent description in our study, as it was found to be invaluable and reliable in modeling the reactivity of solvents with varying polarity.[50]

Two cluster models of graphene comprising of $C_{96}H_{24}$ and $C_{294}H_{42}$ atoms were considered to investigate the substrate-induced effect on the adsorption $(Gua)_n$ bases. Although molecular adsorption on 2D materials typically employs periodic calculations mimicking the characteristics of an infinite slab, cluster models can provide reliable descriptions to localized interactions like adsorption[51,52] and core level shifts.[53] The convergence of interaction energy, interplanar distance, HOMO–LUMO energy gap and dipole moments as a function of cluster size was investigated previously,[46] and as expected, the binding energies are converged with an increase in the cluster size while the HOMO–LUMO energy gap decreases with an increase in the cluster size.[46,54] Although a graphene ($X_{54}H_{18}$) cluster was proven to be effective for proton transport,[55] larger clusters were considered to further reduce the edge effects influencing the energetics of interaction. Note that comparison of our results for the Gua/graphene complex with those obtained using the periodic supercell method within the framework of local, semi-local, and vdW-corrected DFT shows excellent agreement (−0.72 eV for LDA, −0.14 eV for PBE and −1.18 eV for PBE + vdW) supporting the accuracy and reliability of the cluster model in describing the local properties such as molecular adsorption.[56]

III. Results and discussion

A. $(Gua)_n$ bases: structure and stability

$(Gua)_n$ bases can assume myriad conformations and diverse polymorphic structures dominated by either bifurcated or intermolecular H-bonds. A bifurcated H-bond is defined as a three-center bond wherein an electronegative atom (mostly oxygen) is bound by two H atoms lying in or close to the plane delimited by them.[57–59] The bifurcated H-bonds constitute about 20–25% of all H-bonds in biological molecules and have been characterized by X-ray diffraction measurements.[60–62] Although the terminology the '*three-centered*' bifurcated H-bond is more prevalent in systems where an H atom is covalently bonded to one electronegative atom and H-bonded to the other two, it has been adopted in explaining other three-centered bonds as well.[63] Conversely, an intermolecular H-bond exists between two interacting molecules, but unlike the bifurcated H-bond it represents atom to atom interaction between the donor and acceptor moieties in a molecular system.

The equilibrium configurations of $(Gua)_n$ bases (for n = 2–6) were obtained by performing an extensive conformational search considering several initial configurations corresponding to stacked and aligned orientations without imposing any symmetry constraint. Some of the initial configurations corresponding to aligned orientations were adopted from a previous DFT study.[34] We find that the equilibrium configurations of $(Gua)_n$ bases are stabilized by an interplay between intermolecular and bifurcated H-bonds. The stacked and aligned configurations of $(Gua)_2$ and $(Gua)_4$ are found to be nearly degenerate (ESI,† Table S1) and difference between stacked and aligned structures are noticeable for $(Gua)_6$.

In the gas phase, $(Gua)_2$ is found to be nonplanar stabilized by two bifurcated H-bonds between N_1–H, N_2–H and O_6 atoms at the PBE-D2 level of theory (Fig. 2a). Since O_6 is in proximity to N_1–H as opposed to N_2–H at an (average) $R_{O–H}$ distance of 1.69 Å, there exists variation in H-bond distances within the bifurcated bond of the dimer. In the solvent phase, $(Gua)_2$ is stabilized by intermolecular H-bonds with an $R_{O–H}$ distance of 1.82 Å (Fig. 3a and Table 1). Here, two O_6 atoms lie in proximity at an $R_{O–O}$ distance of 3.40 Å. However, in the gas phase, due to large degrees of freedom and molecular flexibility, $(Gua)_2$ adopts an anti-parallel configuration minimizing the steric repulsion between the O-atoms in the dimer.

$(Gua)_3$ prefers a partial cage-like structure stabilized by three bifurcated H-bonds between the N_1–H, N_2–H and O_6 atoms in both gas and solvent phases (Fig. 2b and 3b). The (average) intermolecular $R_{O–H}$ distance is 1.83 (1.81) Å in the gas (solvent) phase. Interestingly, for configurations stabilized *via* bifurcated H-bonds, a 6-membered pyrimidine ring solely participates in the base–base interactions and a 5-membered imidazole ring remains mostly inaccessible. This may be due to the sharing of the pyrimidine ring coupled with the inclusion of vdW dispersion interaction that leads to puckering of the configuration which maximizes the '*long-range*' interactions.

In $(Gua)_4$, transition to a near-planar configuration (Fig. 2c) is predicted which is stabilized by intermolecular H-bonds. The quartet has an inner diameter of 6.88 Å and an (average) intermolecular $R_{O–H}$ distance of 1.67 (1.70) Å in the gas (solvent) phase. Our results are in agreement with the B3LYP/6-31G(d,p) results[64] reporting $(Gua)_4$ with S_4 symmetry to be the stable one. The $R_{O–H}$ and $R_{N–H}$ H-bond distances were comparable at the S_4 symmetry and inclusion of D2 correction results in shortening of H-bond lengths and stabilization of the quartet. Furthermore,

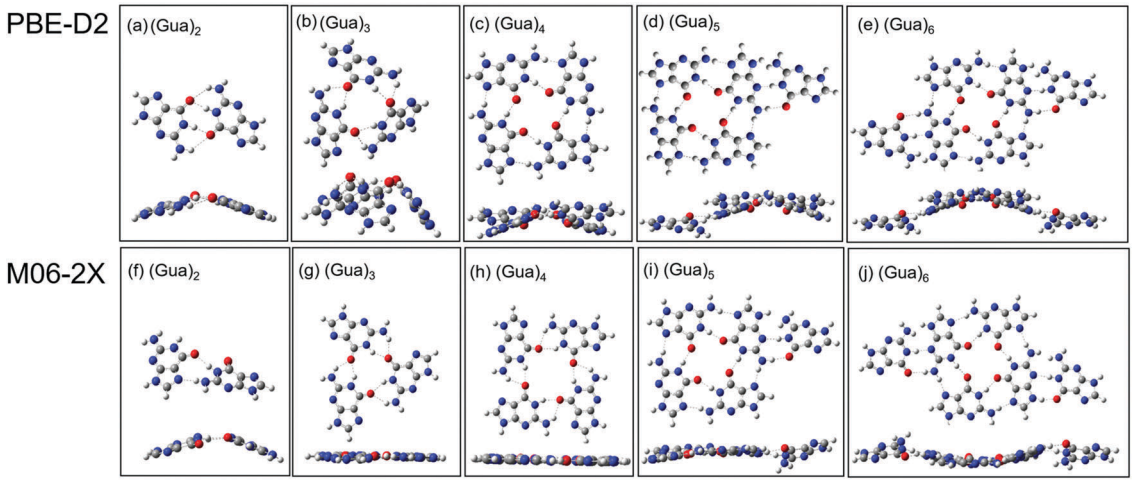

Fig. 2 Gas-phase equilibrium configurations of $(Gua)_n$ bases obtained at the (a–e) dispersion-corrected PBE-D2, and (f–j) hybrid meta-GGA M06-2X levels of theory.

Table 1 $(Gua)_n$ bases with n = 2–6: point group symmetry, binding energy (E_b), binding energy per base (E_b/n), and (average) intermolecular R_{O-H} distance calculated at the dispersion-corrected PBE-D2 and the hybrid meta-GGA M06-2X levels of theory. $E_b = E_{(Gua)_n} - nE_{Gua}$, where n is the number of Gua bases and E is the total energy of the system

	Dispersion-corrected PBE-D2			Hybrid meta-GGA M06-2X			
	Symmetry	E_b (eV)	E_b/n (eV)	R_{O-H} (Å)	Symmetry	E_b (eV)	E_b/n (eV)	R_{O-H} (Å)
Gas phase								
$(Gua)_2$	C_2	−1.48	−0.74	1.69	C_1	−0.55	−0.28	1.90
$(Gua)_3$	C_3	−3.04	−1.0	1.83	C_3	−2.43	−0.81	1.85
$(Gua)_4$	S_4	−4.29	−1.07	1.67	C_4	−3.45	−0.86	1.89
$(Gua)_5$	C_1	−5.41	−1.08	1.72	C_1	−4.17	−0.83	1.78
$(Gua)_6$	C_2	−6.53	−1.09	1.75	C_1	−4.43	−0.74	1.75
Solvent phase								
$(Gua)_2$	C_1	−0.72	−0.36	1.82	C_1	−0.44	−0.22	1.87
$(Gua)_3$	C_1	−1.89	−0.63	1.81	C_1	−1.16	−0.39	1.86
$(Gua)_4$	S_4	−3.12	−0.78	1.70	C_4	−1.62	−0.41	1.89
$(Gua)_5$	C_1	−3.94	−0.79	1.74	C_1	−2.24	−0.45	1.85
$(Gua)_6$	C_2	−4.73	−0.79	1.77	C_1	−2.55	−0.43	1.77

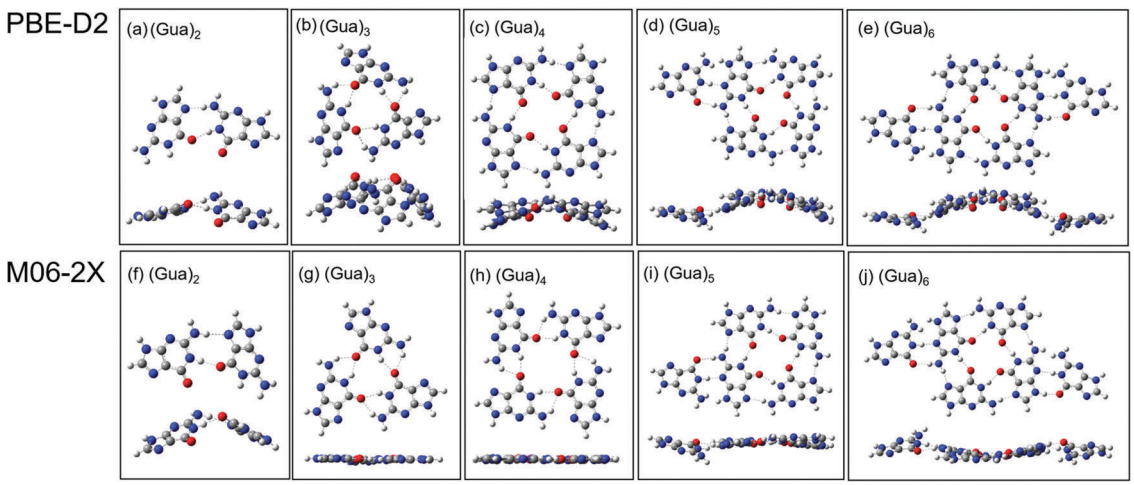

Fig. 3 Solvent-phase equilibrium configurations of $(Gua)_n$ bases obtained at the (a–e) dispersion-corrected PBE-D2 and (f–j) hybrid meta-GGA M06-2X levels of theory.

we find that the planar $(Gua)_4$ stabilized by bifurcated H-bonds is higher in energy ($\sim$0.5 eV) than the near-planar $(Gua)_4$ at the PBE-D2 level of theory.

In $(Gua)_5$ and $(Gua)_6$, the intermolecular H-bonds stabilize the complexes in both gas (Fig. 2d and e) and solvent (Fig. 3d and e) phases. The (average) R_{O-H} within the quartet is calculated to be $\sim$1.68 Å for both bases, consistent with the $(Gua)_4$ quartet, while the additional base is stabilized at an R_{O-H} distance of 1.89 Å. Similarly, in $(Gua)_6$, addition of two bases does not perturb the $(Gua)_4$ quartet configuration ((average) intermolecular R_{O-H} within the quartet = 1.68 Å) and the two bases interact at an (average) R_{O-H} distance of 1.89 Å. In the gas phase, the (average) intermolecular R_{O-H} distances within the $(Gua)_5$ and $(Gua)_6$ complexes are 1.72 and 1.75 Å, respectively. A similar argument holds for the $(Gua)_4$–$(Gua)_6$ complexes in solvent and an inclusion of one or two bases to the $(Gua)_4$ quartet leads to an increase in the intermolecular R_{O-H} distance to 1.89 Å along the extended quartet motif. Compared to $(Gua)_4$ stabilized which is at an (average) R_{O-H} distance of 1.70 Å, additional Gua bases do not perturb the intermolecular R_{O-H} distances within the quartet motif. A detailed list of the bond distances namely, R_{O-H}, R_{O-O}, R_{N-H}, R_{N-N}, and R_{C-C}, is provided in the ESI,† Table S2.

The selectivity and stability of $(Gua)_n$ complexes *via* the formation of bifurcated and/or intermolecular H-bonds has been elucidated as follows. In a bifurcated H-bond complex (*e.g.* Fig. 2a or b), the bases adopt a configuration that minimizes steric repulsion between O_6 atoms, and stabilizes *via* H-bond interactions between N_1–H and N_2–H atoms.[65] For smaller $(Gua)_n$ complexes with $n < 3$, stabilization typically occurs through bifurcated H-bonds. With an increase in the number of bases, intermolecular H-bonds precede the bifurcated H-bond involving interactions through the pyrimidine and imidazole rings. At the PBE-D2 level of theory, $(Gua)_4$, $(Gua)_5$ and $(Gua)_6$ bases interact preferentially through intermolecular H-bonds maximizing the involvement of both electron donor and acceptor moieties of Gua. It is to be noted that the energy difference between $(Gua)_4$ quartets consisting of bifurcated or intermolecular H-bonds is quite small ($\approx$1–5 meV) at the Hartree–Fock (HF) and hybrid B3LYP levels of theory.[66] Overall, a large degree of flexibility towards base–base interactions facilitate molecular stability *via* bifurcated and/or intermolecular H-bonds in smaller $(Gua)_n$ bases. With an increase in the number of bases beyond $(Gua)_4$, constraint in molecular geometry coupled with the association of 6 + 5 membered rings within the base maximizes the stability *via* intermolecular H-bonds.

The calculated binding energy of $(Gua)_n$ in gas and solvent phases is listed in Table 1 at the PBE-D2 and M06-2X levels of theory. In the gas phase, the calculated binding energy/base is −0.74, −1.0, −1.07, −1.08 and −1.09 eV for $(Gua)_2$, $(Gua)_3$, $(Gua)_4$, $(Gua)_5$, and $(Gua)_6$, respectively, suggesting the saturation of stabilization of $(Gua)_n$ bases with an increase in the number of homomers. This is also the case in the solvent phase where the binding energy/base is −0.36, −0.63, −0.78, −0.79 and −0.79 eV for $(Gua)_2$, $(Gua)_3$, $(Gua)_4$, $(Gua)_5$, and $(Gua)_6$, respectively. It is to be noted that the calculated binding energy of $(Gua)_2$ is −1.48 eV (−0.72 eV) in the gas (solvent) phase which is comparable to the (Gua–Cyt) base pair with a binding energy of −1.63 eV (−1.16 eV) in the gas (solvent) phase.[67] Thus, the calculated results support a high tendency for Gua dimerization in both gas and solvent phases. Our results are in excellent agreement with the previous reported results obtained at the local density approximation (LDA) with the additional DFT-D correction for the gas-phase $(Gua)_2$ in predicting enhanced stability of an aligned configuration *via* intermolecular H-bonds.[68]

In the framework of the M06-2X level of theory, $(Gua)_2$ prefers a nonplanar configuration stabilized by two intermolecular H-bonds as depicted in Fig. 2f (gas) and Fig. 3f (solvent). The equilibrium configurations of $(Gua)_3$ and $(Gua)_4$ are planar, stabilized solely by three and four bifurcated H-bonds (Fig. 2g and h (gas) and Fig. 3g and h (solvent)). Note that a comparison of the gas-phase equilibrium configurations of the $(Gua)_4$ quartet suggests a strong dependence of the functional form and level of DFT calculations: M06-2X/6-31+G(d,p) predicts planar geometry while M06-2X/cc-pVDZ obtains a nonplanar configuration,[69] although both the complexes are stabilized by four bifurcated H-bonds (Table S2 of the ESI†). $(Gua)_5$ and $(Gua)_6$ bases deviate from planar geometries with puckering of the quartet motif (Fig. 2i, j and 3i, j) and are stabilized by intermolecular H-bonds. Overall, the equilibrium configurations obtained at the M06-2X/6-31+G(d,p) level demonstrate a transition from nonplanar to planar and then puckered geometries in going from $(Gua)_2$ to $(Gua)_6$.

Additional calculations were performed to determine the equilibrium configurations and optimized parameters of $(Gua)_n$ bases at the wB97XD and M05-2X levels of theory as shown in Fig. 4. The results find the equilibrium configurations obtained at the wB97XD level to be nonplanar. $(Gua)_2$ and $(Gua)_3$ are stabilized by bifurcated H-bonds at an average R_{O-H} distance of 1.74 and 1.86 Å, respectively. Beyond $(Gua)_3$, the complexes are stabilized primarily by intermolecular H-bonds with an average R_{O-H} distance between 1.7 and 1.8 Å (see Table S3 of the ESI†).

The meta-hybrid M05-2X functional form also yields a nonplanar configuration for $(Gua)_2$ and $(Gua)_3$ as depicted in Fig. 4f and g. The average R_{O-H} distance of 1.78 and 1.85 Å was calculated for $(Gua)_2$ and $(Gua)_3$, respectively (Table S3 of the ESI†). The calculated results for $(Gua)_3$ were in contrast to the planar configuration obtained at the M06-2X level of theory. The $(Gua)_4$ configuration is found to be perfectly planar with an average R_{O-H} distance of 1.87 Å (see Fig. 4h and Table S3 of the ESI†). In $(Gua)_5$ and $(Gua)_6$, the quartet motif comprising of the four bases is observed to be a near-planar geometry, stabilized *via* intermolecular and bifurcated H-bonds and the orientation of the +1 and +2 bases is offset from planarity as depicted in Fig. 4i and j at an average intermolecular R_{O-H} distance of $\sim$1.90 Å. Thus, dispersion corrected PBE-D2 and wB97XD functional forms yield a similar equilibrium configuration for the bases considered, while variations are observed at the M05-2X and M06-2X levels of theory especially for $(Gua)_3$, $(Gua)_5$ and $(Gua)_6$ complexes. The equilibrium configurations and optimized parameters of $(Gua)_n$ bases at the wB97XD and M05-2X levels of theory corresponding to the solvent phase is shown in Fig. S1 of the ESI.†

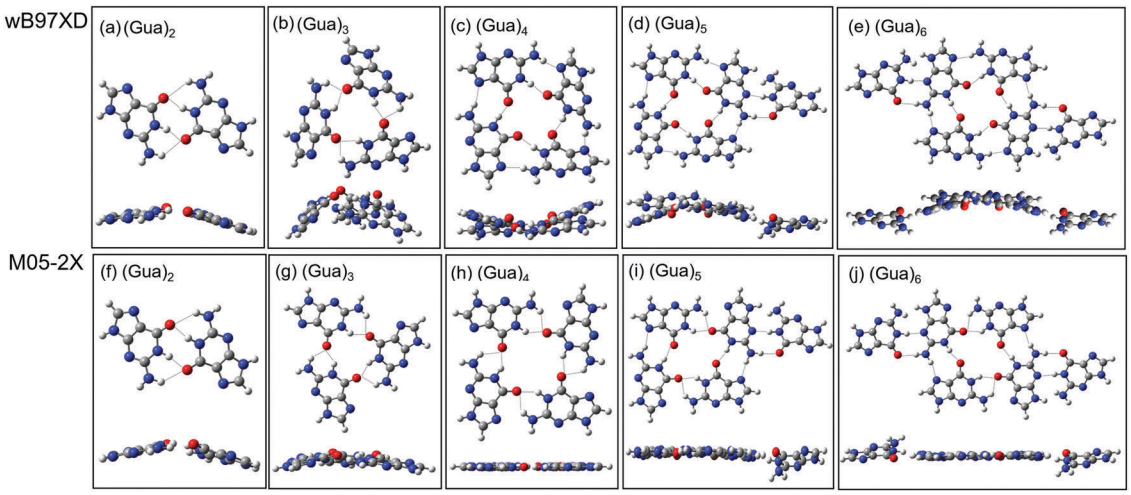

Fig. 4 Gas-phase equilibrium configurations of $(Gua)_n$ bases obtained at the (a–e) dispersion-corrected wB97XD and (f–j) M05-2X levels of theory.

The gas-phase binding energy for $(Gua)_2$ to $(Gua)_6$ is depicted in Fig. 5a. The overall trend in variation of the binding energy follows the order: PBE-D2 > wB97XD > M05-2X > M06-2X. The binding energy/base converges beyond $(Gua)_3$ (Table S3 of the ESI†) suggesting a net per base stabilization of the (Gua) complexes with increase in the number of homomers in both gas and solvent phases.

The relative stability of $(Gua)_n$ defined as the binding energy/H-bonds demonstrates a characteristic trend at the various levels of theory. At the M06-2X and M05-2X levels of theory (Fig. 4b), $(Gua)_4$ has a higher relative stability and is in good agreement with the prior reported results obtained at the B3LYP, M05-2X, M06-2X and RI-DFTD BLYP levels of theory.[18] In contrast, the PBE-D2 and w97XD results show that the stability progressively levels off in going from $(Gua)_4$ to $(Gua)_6$. The RI-DFTD calculations which include the dispersion term demonstrate a similar trend with the DFT-D2 beyond $(Gua)_4$ quartet.[18] The results therefore suggest a substantial dependence of the stability of $(Gua)_n$ bases on the long-range vdW interaction. Likewise, in the solvent phase we find a similar trend in relative stability of $(Gua)_n$ bases as provided in the ESI,† Fig. S2, at the PBE-D2, wB97XD, M05-2X and M06-2X levels of theory.

To further investigate the subtle effects introduced by the way we describe the dispersive term in DFT calculations, we compare the dipole moment values corresponding to the gas phase as illustrated in Fig. 6. At the PBE-D2 level, $(Gua)_2$ and $(Gua)_3$ exhibit dipole moment values of 3.7 and 9.0 Debye which is correlated to the highly-puckered geometry. $(Gua)_4$ has a near-planar geometry compared to $(Gua)_2$ and $(Gua)_3$ with a lower value of dipole moment. The M06-2X functional find both $(Gua)_3$ and $(Gua)_4$ to have planar configurations with dipole moment values of 0.4 and 0.1 Debye, respectively. In contrast, $(Gua)_2$ which is highly puckered and nonplanar has a dipole moment value of 11.5 Debye. Beyond $(Gua)_4$, the transition from planar to nonplanar geometries are reflected in an increase of dipole moment values for $(Gua)_5$ and $(Gua)_6$.

The dipole moment calculated at the wB97XD level is similar to the PBE-D2 values, suggesting a consistent correlation in the equilibrium configuration of (Gua) complexes within the included vdW dispersion. At the M05-2X level, a dipole moment value of ~3.0 Debye for $(Gua)_2$ and $(Gua)_3$ is associated with the nonplanar equilibrium configuration as shown in Fig. 4f and g. In $(Gua)_4$, except at the PBE-D2 level, which yields a dipole moment of 2.5 Debye, the wB97XD, M05-2X and M06-2X functionals predict

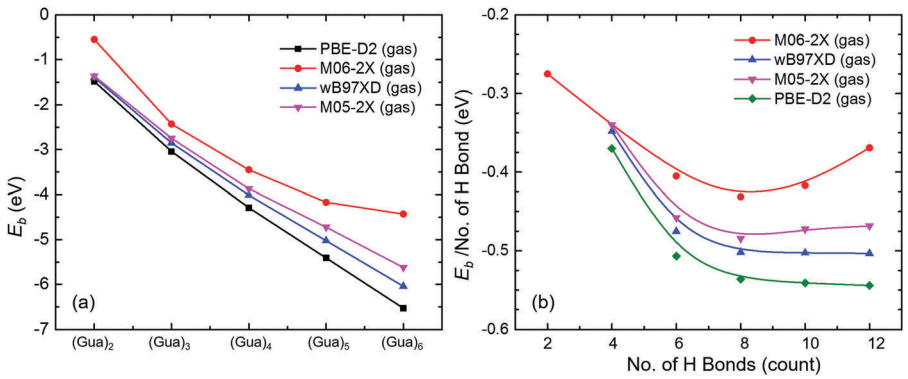

Fig. 5 (a) Calculated binding energies at the dispersion-corrected PBE-D2, wB97XD and hybrid meta-GGA M05-2X, M06-2X levels of theory. (b) Relative stability/H-bond of $(Gua)_n$ bases in the gas phase.

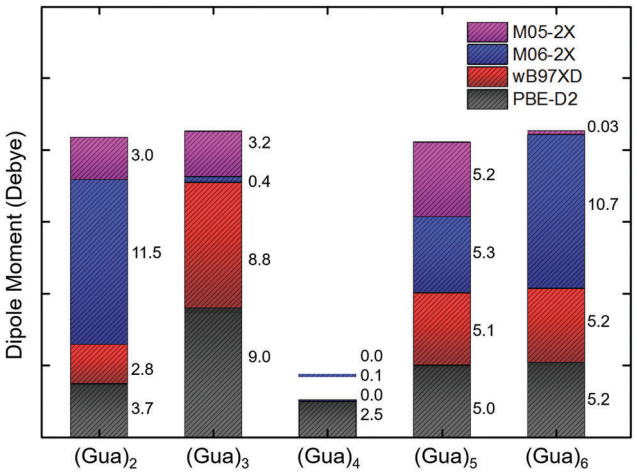

Fig. 6 Calculated dipole moments of $(Gua)_n$ in (a) gas and (b) solvent phases.

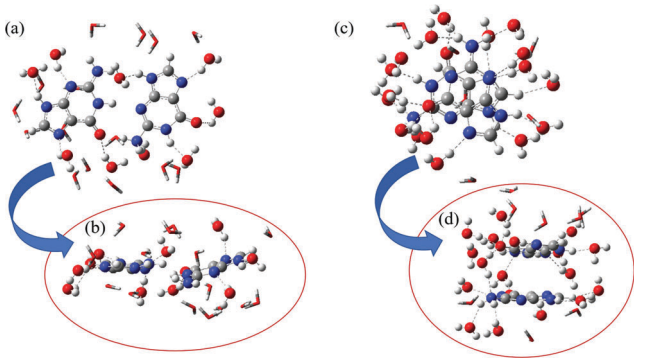

Fig. 7 Top and side views of the water solvation layer in $(Gua)_2$ in (a and b) aligned (c and d) stacked configurations.

a dipole moment of ~0.0 Debye. Although the equilibrium configuration of $(Gua)_4$ at the wB97XD level of theory is puckered, it is perfectly centrosymmetric which is reflected from its zero dipole moment. Likewise, in $(Gua)_6$, the symmetry of the complex with a planar quartet motif results in a small dipole moment of 0.03 Debye. The overall trend in dipole moment in the gas phase supports a good correlation between the wB97XD and PBE-D2 levels of theory while variations are observed at the M0X-2X levels.

The solvent phase calculations find higher values of dipole moment compared to the gas phase values (see the ESI,† Fig. S3) due to the screening of intermolecular interactions as also reflected in isosurface plots of ESP displayed in the ESI,† Fig. S4 and S5. Overall, the results clearly demonstrate the influence of the way we include the vdW dispersion interaction terms in the calculations; the results support the dimerization of $(Gua)_n$, though PBE-D2 results find higher binding energies and slightly smaller intermolecular H-bond distances within the base pairs relative to the other three functionals. Thus, subtle differences in predicting the equilibrium configurations of free-standing $(Gua)_n$ bases under physiological conditions can become quite substantial, as more polar $(Gua)_n$ in the gas phase is likely to exhibit greater stabilization compared to the solvent phase counterparts.

To account for the subtle intermolecular interactions between the Gua bases and water molecules defined explicitly, we considered the case of solvation of $(Gua)_2$ base pairs. Molecular dynamics (MD) simulation on the preferred orientation in interaction of free-standing $(Gua)_n$ bases in gas and solvent phases demonstrate a selectivity in the stabilization of the complexes.[67] The bases interact *via* intermolecular H-bonds in the gas phase while in solvent, screening of intermolecular interaction introduced by water molecules leads to π–π stacked configurations. Fig. 7 illustrates the explicit solvation of $(Gua)_2$ bases in the stacked and aligned configurations, depicting the water hydration layer along the bases, modeled with 24 water molecules for the two configurations considered. The interaction energy of the complex is defined as the difference in the total energy of the combined system and the individual constituents (*i.e.* the total energy of the 24 water molecules and the bases in the stacked and aligned configurations), respectively. Energetically, the stacked configuration (an interaction energy value of −7.63 eV) is preferred over the aligned (an interaction energy of −5.78 eV) and the average interacting distance between water and Gua is calculated to be 1.92 and 1.98 Å in the stacked and aligned configurations, respectively.

The stacked configuration facilitates an increased availability in intermolecular H-bonds with the water molecules and around 18 water molecules constituting the first hydration sphere around the bases as depicted in Fig. 7c. On the other hand, the intermolecular H-bond interaction between the base pairs in the aligned configuration reduces the availability for H-bonding with water molecules and around 9 waters constitute the solvation sphere (Fig. 7b). The enhanced stability of the stacked $(Gua)_2$ dimers demonstrates that the water–water dipolar interactions play an important role in base–base stabilization *via* the screening of intermolecular H-bonded interaction and rendering conformational flexibility towards the association. The comparison of the implicit *vs.* explicit solvation model therefore finds the implicit solvent description to be reliable for the present set of calculations.

B. Adsorption of $(Gua)_n$ bases on graphene

To comprehend the nature, preferentiality and energetics of interaction of $(Gua)_n$ bases with graphene, calculations were performed on (Gua)/graphene, $(Gua)_2$/graphene and $(Gua)_4$/graphene complexes in both gas and solvent phases at the PBE-D2 level. The aim here being to determine the extent to which graphene-induced effects can alter the equilibrium configurations of free-standing $(Gua)_2$ and $(Gua)_4$ complexes. Note that the carbon atoms in graphene are sp^2 hybridized and the out-of-plane C-p_z orbitals form π bonding and π* antibonding orbitals. Analysis of the calculated results in terms of the interaction strength describing the base–surface interaction, inter-base H-bonds and dipole moments describing the polarity of the complexes was considered. The interaction energy between $(Gua)_n$ bases and graphene is defined as the difference in the total energy of the $(Gua)_n$/graphene complex and the total

energies of free-standing $(Gua)_n$ bases and graphene. It is to be noted that the availability of multiple interacting sites in $(Gua)_n$ bases introduces a complex energy landscape relative to the case of a single base molecule interacting with graphene. For a single Gua molecule physisorbed on graphene (ESI,† Fig. S6), the parallel stacked base–substrate configuration is preferred at an interplanar distance of ~3.12 (~3.15) Å in the gas (solvent) phase. The calculated interaction energy of −1.02 (−0.82) eV in the gas (solvent) phase (see Table S4 of the ESI†) suggests significant screening of the interaction strength in solvents.

Fig. 8a and b depict the calculated minimum energy configurations of $(Gua)_2$/graphene in gas and solvent phases. The $(Gua)_2$ bases are perfectly aligned along graphene at an average interplanar distance of ~3.12 (~3.15) Å in the gas (solvent) phase. The interaction energy of the aligned $(Gua)_2$/graphene complex is −1.72 (−1.58) eV in the gas (solvent) phase and (average) the intermolecular R_{O-H} distance between the bases is calculated to be 1.66 (1.67) Å in the gas (solvent) phase. On the other hand, for the stacked $(Gua)_2$/graphene configuration (ESI,† Fig. S7a and b), the calculated interaction energy is −1.04 (−0.88) eV in the gas (solvent) phase with a base–base stacking distance of ~2.95 Å. The calculated interplanar distance between $(Gua)_2$ and graphene is about ~3.12 (~3.14) Å in the gas (solvent) phase. Here, the second Gua base is under the influence of the adjacent base and does not sense the effect of graphene in the stacked mode of adsorption. Thus, the stacked $(Gua)_2$/graphene configuration mimics the case of a Gua/graphene complex in having a similar interaction strength in both gas and solvent phases.

The preferred mode of interaction of $(Gua)_2$ on graphene is found to be the aligned configuration, though the difference in the total energy for the stacked and aligned configurations is relatively small (~1 eV) as shown in Table 2. Unlike the free-standing $(Gua)_2$ which prefers a nonplanar (puckered) configuration (Fig. 2a and 3a), adsorption on graphene leads to the near planar geometries. This is due to the influence of the graphene substrate wherein planar geometries facilitate maximum overlap of π-orbitals associated with the interacting moieties (Fig. 8a and b). Interestingly, the solvent phase results show a noticeable decrease in the (average) intermolecular R_{O-H} distance from 1.82 (free-standing) to 1.67 Å suggesting enhanced base–base intermolecular interaction, though the gas phase results find very small graphene-induced effects with the (average) H-bond distance decreasing from 1.69 (free-standing) to 1.66 Å.

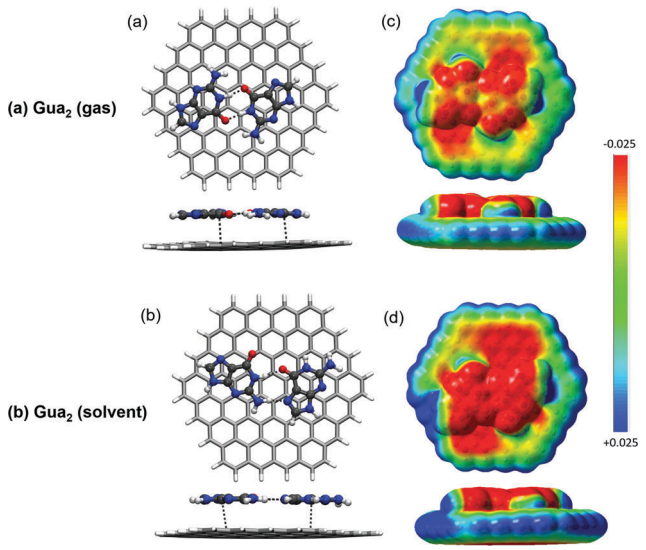

Fig. 8 Calculated equilibrium configuration and ESP isosurface plots of $(Gua)_2$/graphene at the aligned configuration in gas and solvent phases.

Furthermore, the significant decrease in polarity of the bases induced by graphene is highlighted in the calculated dipole moments and isosurface of ESP along the interaction region. For example, the dipole moment of the aligned $(Gua)_2$/graphene complex is 2.0 (2.5) Debye in the gas (solvent) phase, while it is 3.7 (15.0) Debye for free-standing $(Gua)_2$ bases in the gas (solvent) phase. The ESP isosurface along the interacting region displays negative charge density along (Gua) with localized contributions on graphene in the gas phase (Fig. 8c). In the presence of solvent (Fig. 8d), regions of negative charge density are further delocalized on graphene and the bases suggesting a redistribution of charge densities along the interacting region. Therefore, graphene-induced stability in molecular geometry appears to lower the polarity of the $(Gua)_2$ base in both gas and solvent phases fulfilling one of the prerequisite criteria for self-assembly of bases on graphene.

The $(Gua)_4$ quartets in both the aligned and stacked configurations were considered for adsorption on graphene. The aligned mode of interaction was preferred on graphene (Fig. 9a and b) and the bases were physisorbed at an interplanar distance of 3.16 (3.19) Å in the gas (solvent) phase (see Table 2). The calculated energy difference between the aligned and stacked $(Gua)_4$/graphene is ~1.3 (~1.4) eV in the gas (solvent) phase.

The graphene-induced effect on the intermolecular H-bond distances within $(Gua)_4$ is minimal; the (average) R_{O-H} distance is calculated to be 1.72 (1.75) Å in the gas (solvent) phase as compared to 1.67 (1.70) Å in the gas (solvent) phase for the free-standing $(Gua)_4$. On the other hand, graphene appears to lower the polarity of free-standing $(Gua)_4$. The dipole moment of aligned $(Gua)_4$/graphene is calculated to be 1.34 (1.89) Debye in the gas (solvent) phase whereas that for free-standing $(Gua)_4$ is 2.5 (3.1) Debye in the gas (solvent) phase. The decrease in polarity can be related to the conformational relaxation within the quartet with an increase in intermolecular H-bond distance and change in the structure from puckered (nonplanar) to near-planar in the presence of the substrate. The ESP isosurface plots (Fig. 9c and d) demonstrate the regions of high (negative) charge density delocalized along the quartet with intermediate charge densities on graphene. Overall, graphene stabilizes the $(Gua)_4$ quartet facilitating conditions for monolayer self-assembly *via* the base–substrate π-stacking interactions without perturbing the structural properties in either the gas or the solvent phase.

To investigate the effect of charges on the hydrogen edge atoms of the graphene cluster on the net interaction energy, we considered a relatively larger graphene nanoflake (modeled with 336 atoms) as depicted in Fig. 10a. The pristine graphene nanoflake has a D_{6h} symmetry and 0 dipole moment value like the

Table 2 $(Gua)_n$/graphene: total energy, interaction energy (E_{int}), BSSE corrected interaction energy, interplanar distance between $(Gua)_n$ bases and graphene, and dipole moment calculated at the PBE-D2 level of theory. E_{int} is calculated as $E_{int} = E_{((Gua)_n/graphene)} - E_{(Gua)_n} - E_{graphene}$ where E is the total energy of the system

System		Total energy (a.u.)	E_{int} (eV)	E_{int} (BSSE corrected) (eV)	Interplanar distance (Å)	Dipole moment (Debye)
Gas phase						
$(Gua)_2$/graphene	Stacked	−4753.2342	−1.04	−0.80	3.12	4.66
	Aligned	−4753.2781	−1.72	−1.18	3.12	2.03
$(Gua)_4$/graphene	Stacked	−5837.3356	−1.65	−1.19	3.11	1.27
	Aligned	−5837.3824	−2.97	−2.04	3.16	1.34
Solvent phase						
$(Gua)_2$/graphene	Stacked	−4753.2765	−0.88	—	3.14	8.20
	Aligned	−4753.3143	−1.58	—	3.15	2.52
$(Gua)_4$/graphene	Stacked	−5837.3877	−1.59	—	3.13	1.21
	Aligned	−5837.4384	−2.79	—	3.19	1.89

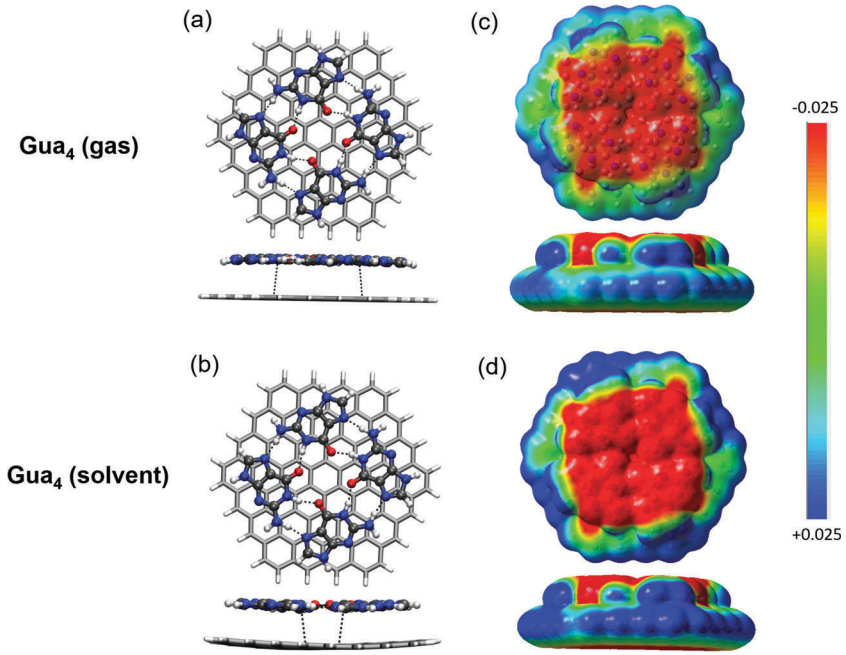

Fig. 9 Calculated equilibrium configuration and ESP isosurface of $(Gua)_4$/graphene in gas and solvent phases.

smaller 120 atom cluster. Since the trends in variation of interaction energy suggest the preferentiality of aligned over the stacked configuration of the bases on graphene, we investigated the physisorption of $(Gua)_4$ in the aligned configuration, as shown in Fig. 10b and c corresponding to the gas and solvent phases.

The adsorption on graphene leads to the formation of planar geometries of $(Gua)_4$ at an average interplanar distance of ~3.17 (3.19) Å in gas (solvent) phases. The interaction energy is calculated to be −3.34 (−3.04) eV in gas (solvent) phases suggesting a net screening of intermolecular interactions in the solvent phase. Monolayer adsorption of $(Gua)_4$ in the aligned configuration maximizes the π-orbital overlap facilitating enhanced intermolecular interactions with significantly reduced edge effects from the H atoms.

C. Effect of BSSE correction on $(Gua)_n$/graphene complexes

In the weakly bound physisorbed complexes governed by noncovalent π–π stacking, *e.g.* $(Gua)_n$/graphene one often encounters an artificial shortening in intermolecular distances and strengthening of the intermolecular interaction, referred to as a basis set superposition error (BSSE). The BSSE generally arises when the wavefunction of a monomer is expanded with a less basis function than the wavefunction of the complex. This accessibility of extra basis function arises because of the inconsistent treatment of the monomers.[70] For molecular complexes separated at a small intermolecular distance, the monomer units can realize the access extra functions from the other monomer, which does not hold for systems separated by larger distances. The counterpoise correction as proposed by Boys and Bernardi[71] determines a correction term, by using the same basis set for the minimum energy configurations of the complex and the individual monomer units (here $(Gua)_n$ and graphene).

We performed the BSSE calculations using the GAUSSIAN09 program suite at the optimized configurations represented in Fig. 8–10, respectively. The BSSE corrected interaction energies were compared with the non-corrected values as shown in Table 2.

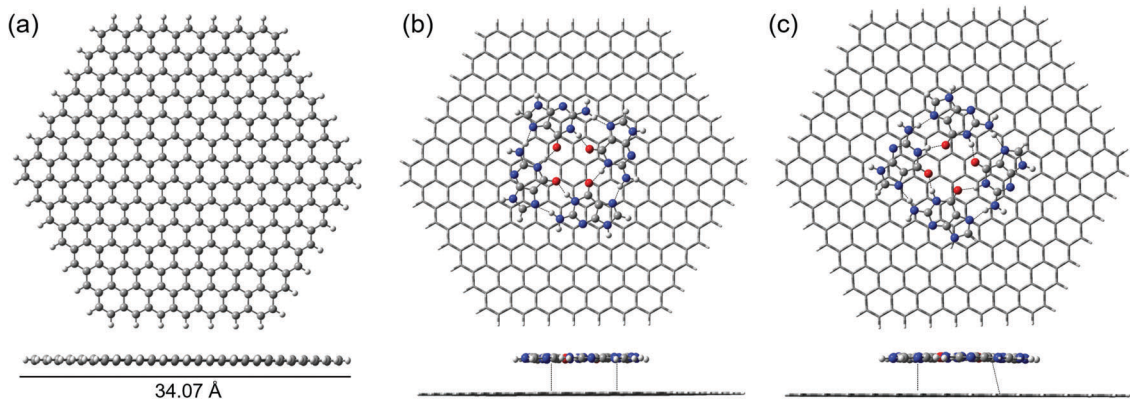

Fig. 10 Calculated equilibrium configuration of (a) graphene nanoflakes consisting of 336 atoms, $(Gua)_4$/graphene nanoflakes in (b) gas and (c) solvent phases.

The trend in the non-corrected interaction energy follows a similar order to those of the BSSE corrected DFT-D calculations:

$(Gua)_2$/graphene: aligned > stacked

$(Gua)_4$/graphene: aligned > stacked

The inclusion of counterpoise correction yields comparatively lower interaction energies in the gas phase and vary in the range of −0.74 to −2.04 eV, suggesting that BSSE plays a vital role in adequately describing the energetics of interaction of $(Gua)_n$/graphene complexes. The trends in BSSE corrected interaction energies suggest that the aligned configurations facilitate an enhanced stabilization of the (Gua) bases by maximizing the orbital overlap with graphene. For the larger graphene nanoflake considered corresponding to the $(Gua)_4$/graphene complex in the gas phase (Fig. 10b), and the BSSE corrected interaction energy is calculated to be −2.34 eV.

The nature of H-bonding in substrate-stabilized $(Gua)_2$ and $(Gua)_4$ bases was compared with that in free-standing bases to gain insights into the substrate-induced effects. $(Gua)_2$ bases adsorbed on graphene (Fig. 8a and b) is stabilized by intermolecular H-bonds within the dimer. We notice that transition from puckered nonplanar to planar configurations is realized due to the substrate induced effect. Unlike the observance of bifurcated (gas phase) and intermolecular (solvent phase) H-bonds in $(Gua)_2$, only intermolecular H-bonds stabilize the complex in the presence of graphene. Likewise, intermolecular H-bond stabilizes the $(Gua)_4$ quartet adsorbed on graphene in both gas and solvent phases. In contrast, stabilization in the stacked configuration of $(Gua)_2$/graphene occurs *via* the base–base and base–substrate interactions (ESI,† Fig. S8). Thus, the monolayer adsorption of Gua bases in the aligned configuration on graphene is preferred from the energetics perspective compared to stacked conformations.

Experimental studies on the self-assembly of Gua oligomers on the graphite surface suggest planar assembly of Gua stabilized by intermolecular H-bonds,[72] and are governed by centrosymmetric dimers the H-bonded interactions.[73] Molecular dynamics (MD) simulation on adsorption of DNA base pairs on graphite find the dimer stabilization to be dominated by H-bonded interactions and follows the order: Gua–Cyt > Ade–Gua > Ade–Thy > Ade–Ade > Cyt–Thy > Gua–Gua > Cyt–Cyt > Ade–Cyt > Thy–Thy > Gua–Thy.[74] Furthermore, MD studies on the adsorption of DNA nucleobases on single walled carbon nanotubes reported that the bases are stabilized by vdW interaction.[75] However, for a charged nanotube surface, the competition between the polarized water and bases results in base–base π-stacking and the bases no longer assemble along the nanotube sidewall. In our study, dispersion-corrected DFT calculations demonstrate that the base pairs and quartets adsorb/assemble in nearly planar geometries along graphene by reducing their individual polarity and maximizing the vdW interactions *via* base–surface π-stacking in both gas and solvent phases.

IV. Summary

Intermolecular interactions governing the self-assembly of $(Gua)_n$ bases are investigated at the level of dispersion-corrected DFT. The calculated results demonstrate that the assembly of free-standing $(Gua)_n$ bases is mainly determined by the base–base intermolecular interactions and influenced by the way we describe the dispersive interactions in DFT calculations. Bifurcated and intermolecular H-bonds typically stabilize the $(Gua)_n$ bases. At the M06-2X level of theory, $(Gua)_n$ bases stabilized *via* bifurcated H-bonds yield nearly planar geometries while bases stabilized by intermolecular H-bonds result in the puckered geometries. The PBE-D2 and wB7XD results find the energetically preferred configurations to have puckered geometries except for $(Gua)_3$ which exhibits a partial cage-like geometry. The substrate-induced effects on the assembly of $(Gua)_n$ bases are associated with coupling of base–base and base–substrate intermolecular interactions. The presence of graphene leads to considerable stabilization of free-standing $(Gua)_n$ bases *via* lowering of the polarity of the bases. A preference for planar geometries by $(Gua)_n$ bases on graphene illustrates the role of substrates in molecular adsorption and stability of $(Gua)_n$ bases. The ESP isosurface provides a detailed representation to the distribution of molecular charge densities on adsorption of the $(Gua)_n$ complexes on graphene.

The subtle influence on the nature of adsorption and the overall stability of $(Gua)_n$ complexes is also determined by the way we model the 2D substrate. Herein, considering the computational limitations in simulating a graphite substrate, we proceed with a monolayer graphene cluster model with constraints applied on the graphene atoms, to mimic a graphite substrate. For the graphene cluster considered, the DFT-D2 results suggest an overall stability of the $(Gua)_n$ complexes in gas and solvent phases and substrate induced monolayer adsorption of the bases compared to the free-standing counterparts. We comprehend that the observed trends would hold for graphite as well in driving the monolayer assembly process. The differences that may be expected are in the energetics of interaction in the conjugated complexes, while the overall essence of interaction will remain the same.

Our results based on dispersion corrected DFT calculations form a basis for atomistic MD simulations of free-standing and interacting $(Gua)_n$ bases in gas and solvent phases. In particular, the MD simulation takes into consideration the high surface coverage density of $(Gua)_n$ bases on graphene to determine the dominate interaction modes namely the base–base *vs.* base–substrate π-stacking, governing the supramolecular self-assembly at the solid/liquid interface.

Competing financial interest

The authors declare no competing financial interest.

Acknowledgements

The authors kindly appreciate the valuable advice and suggestions from Prof. Max Seel. Helpful discussions with K. Waters, G. Wang and Dr S. Gowtham are kindly acknowledged. NS acknowledges financial support and funding from Michigan Technological University, Houghton, MI. Computational resources at Michigan Technological University with the SUPERIOR high-performance computing cluster were utilized in the study. This research is partially supported by the Army Research Office through grant number W911NF-14-2-0088.

References

1 W.-W. Zhao, J.-J. Xu and H.-Y. Chen, *Chem. Rev.*, 2014, **114**, 7421.
2 Y. Hee Jang, W. A. Goddard III, K. T. Noyes, L. C. Sowers, S. Hwang and D. S. Chung, *J. Phys. Chem. B*, 2003, **107**, 344.
3 C. A. M. Seidel, A. Schulz and M. H. M. Sauer, *J. Phys. Chem.*, 1996, **100**, 5541.
4 M. Preuss, W. G. Schmidt, K. Seino, J. Furthmuller and F. Bechstedt, *J. Comput. Chem.*, 2004, **25**, 112.
5 S. D. Wetmore, R. J. Boyd and L. A. Eriksson, *Chem. Phys. Lett.*, 2000, **322**, 129.
6 N. B. Leontis, J. Stombaugh and E. Westhof, *Nucleic Acids Res.*, 2002, **30**, 3497.
7 D. Bhattacharyya, S. Koripella, A. Mitra, V. Rajendran and B. Sinha, *J. Biosci.*, 2007, **32**, 809.
8 J. Gros, F. Rosu, S. Amrane, A. De Cian, V. Gabelica, L. Lacroix and J.-L. Mergny, *Nucleic Acids Res.*, 2007, **35**, 3064.
9 S. M. Douglas, H. Dietz, T. Liedl, B. Hogberg, F. Graf and W. M. Shih, *Nature*, 2009, **459**, 414.
10 N. Hastie, M. Dempster, M. Dunlop, A. Thompson, D. Green and R. Allshire, *Nature*, 1990, **346**, 866.
11 *Data for Biochemical Research*, ed. R. M. C. Dawson, W. H. Elliot and K. M. Jones, Clarendon Press, Oxford, U.K., 3rd edn, 1986.
12 Y. Li, M. Dong, D. E. Otzen, Y. Yao, B. Liu, F. Besenbacher and W. Mamdouh, *Langmuir*, 2009, **25**, 13432.
13 H. Tanaka and T. Kawai, *Mater. Sci. Eng., C*, 1995, **3**, 143.
14 N. Borovok, T. Molotsky, J. Ghabboun, D. Porath and A. Kotlyar, *Anal. Biochem.*, 2008, **374**, 71.
15 N. J. Tao, J. A. Derose and S. M. Lindsay, *J. Phys. Chem.*, 1993, **97**, 910.
16 I. Yoshikawa, J. Sawayama and K. Araki, *Angew. Chem., Int. Ed.*, 2008, **47**, 1038.
17 S. Sivakova and S. J. Rowan, *Chem. Soc. Rev.*, 2005, **34**, 9.
18 A. K. Jissy, U. P. M. Ashik and A. Datta, *J. Phys. Chem. C*, 2011, **115**, 12530.
19 J. Gu and J. Leszczynski, *J. Phys. Chem. A*, 2000, **104**, 6308.
20 R. Otero, J. M. Gallero, A. L. Vazquez de Parga, N. Martin and R. Miranda, *Adv. Mater.*, 2011, **23**, 5148.
21 A. Ciesielski and P. Samori, *Adv. Mater.*, 2016, **28**, 6030.
22 L. Liu, D. Xia, L. H. Klausen and M. Dong, *Int. J. Mol.*, 2014, **15**, 1901.
23 D. G. Reuven, H. B. M. Shashikala, S. Mandal, M. N. V. Williams, J. Chaudhary and X.-Q. Wang, *J. Mater. Chem. B*, 2013, **1**, 3926.
24 A.-M. Chiorcea and A. M. Oliveira-Brett, *Bioelectrochemistry*, 2002, **55**, 63.
25 J. E. Freund, M. Edelwirth, P. Krobel and W. M. Heckl, *Phys. Rev. B: Condens. Matter Mater. Phys.*, 1997, **55**, 5394.
26 D. Akinwande, N. Petrone and J. Hone, *Nat. Commun.*, 2014, **5**, 5678.
27 E. G. Hohenstein, S. T. Chill and C. D. Sherrill, *J. Chem. Theory Comput.*, 2008, **4**, 1996.
28 P. de Silva, T. Zhu and T. V. Voorhis, *J. Chem. Phys.*, 2017, **146**, 024111.
29 L. A. Burns, Á. Vázquez-Mayagoitia, B. G. Sumpter and C. D. Sherrill, *J. Chem. Phys.*, 2011, **134**, 084107.
30 N. Marom, A. Tkatchenko, M. Rossi, V. V. Gobre, O. Hod, M. Scheffler and L. Kronik, *J. Chem. Theory Comput.*, 2011, **7**, 3944.
31 E. R. Johnson and A. D. Becke, *J. Chem. Phys.*, 2005, **123**, 024101.
32 S. Grimme, *J. Comput. Chem.*, 2006, **27**, 1787.
33 A. K. Jissy and A. Datta, *J. Phys. Chem. Lett.*, 2014, **5**, 154.
34 Y. Zhao and D. G. Truhlar, *J. Chem. Theory Comput.*, 2007, **3**, 289.
35 W. Reckien, F. Janetzko, M. F. Peintinger and T. Bredow, *J. Comput. Chem.*, 2012, **33**, 2023.
36 S. Grimme, J. Antony, S. Ehrlich and H. Krieg, *J. Chem. Phys.*, 2010, **132**, 154104.

37 Q. Wu and W. Yang, *J. Chem. Phys.*, 2002, **116**, 515.
38 S. Grimme, *J. Comput. Chem.*, 2004, **25**, 1463.
39 Y. Zhao and D. G. Truhlar, *Theor. Chem. Acc.*, 2008, **120**, 215.
40 J. P. Perdew, K. Burke and Y. Wang, *Phys. Rev. B: Condens. Matter Mater. Phys.*, 1996, **54**, 16533.
41 M. S. Gordon, *Chem. Phys. Lett.*, 1980, **76**, 163.
42 P. Zhang, X. Hou, J. Mi, Y. He, L. Lin, Q. Jiang and M. Dong, *Phys. Chem. Chem. Phys.*, 2014, **16**, 17479.
43 A. J. Cohen, P. Mori-Sánchez and W. T. Yang, *Chem. Rev.*, 2012, **112**, 289.
44 W. Wang, Y. Zhang and Y.-B. Wang, *J. Chem. Phys.*, 2014, **140**, 094302.
45 D. Le, A. Kara, E. Schröder, P. Hyldgaard and T. S Rahman, *J. Phys.: Condens. Matter*, 2012, **24**, 424210.
46 N. Saikia, M. Seel and R. Pandey, *J. Phys. Chem. C*, 2016, **120**, 20323.
47 K. Waters, R. Pandey and S. P. Karna, *ACS Omega*, 2017, **2**, 76.
48 M. J. Frisch, G. W. Trucks, H. B. Schlegel, G. E. Scuseria, M. A. Robb, J. R. Cheeseman, G. Scalmani, V. Barone, B. Mennucci and G. A. Petersson, *et al.*, *Gaussian 09*, Gaussian, Inc., Wallingford, CT, 2009.
49 J. Tomasi, B. Mennucci and R. Cammi, *Chem. Rev.*, 2005, **105**, 2999.
50 R. E. Skyner, J. L. McDonagh, C. R. Groom, T. van Mourik and J. B. O. Mitchell, *Phys. Chem. Chem. Phys.*, 2015, **17**, 6174.
51 M. Seel and P. S. Bagus, *Phys. Rev. B: Condens. Matter Mater. Phys.*, 1981, **23**, 5464.
52 M. Seel and P. S. Bagus, *Phys. Rev. B: Condens. Matter Mater. Phys.*, 1983, **28**, 2023.
53 P. S. Bagus and M. Seel, *Phys. Rev. B: Condens. Matter Mater. Phys.*, 1981, **23**, 2065.
54 U. Saikia, N. Saikia, K. Waters, R. Pandey and M. B. Sahariah, *ChemistrySelect*, 2017, **2**, 3613–3621.
55 M. Seel and R. Pandey, Proton and hydrogen transport through two-dimensional monolayers, *2D Mater.*, 2016, **3**, 025004.
56 J.-H. Lee, Y.-K. Choi, H.-J. Kim, R. H. Scheicher and J.-H. Cho, *J. Phys. Chem. C*, 2013, **117**, 13435.
57 G. A. Jeffrey, *An Introduction to Hydrogen Bonding*, Oxford University Press, New York, 1997.
58 G. R. Desiraju and T. Steiner, *The Weak Hydrogen Bond in Structural Chemistry and Biology*, Oxford University Press, New York, 1999.
59 R. D. Parra, M. Furukawa, B. Gong and X. C. Zeng, *J. Chem. Phys.*, 2001, **115**, 6030.
60 R. E. Marsh, *Acta Crystallogr.*, 1958, **11**, 654.
61 R. Parthasarathy, *Acta Crystallogr., Sect. B: Struct. Crystallogr. Cryst. Chem.*, 1969, **25**, 509.
62 R. Preißner, U. Egner and W. Saenger, *FEBS Lett.*, 1991, **288**, 192.
63 I. Rozas, I. Alkorta and J. Elguero, *J. Phys. Chem. A*, 1998, **102**, 9925.
64 M. Meyer, T. Steinke, M. Brandl and J. Sühnel, *J. Comput. Chem.*, 2001, **22**, 109.
65 J. Gu, J. Leszczynski and M. Bansal, *Chem. Phys. Lett.*, 1999, **311**, 209.
66 M. Meyer, M. Brandl and J. Suhnel, *J. Phys. Chem. A*, 2001, **105**, 8223.
67 N. Saikia, K. Waters, S. Karna and R. Pandey, *ACS Omega*, 2017, in review.
68 N. Ding, X. Chen, C.-M. L. Wu and H. Li, *Phys. Chem. Chem. Phys.*, 2013, **15**, 10767.
69 G. Villani, *New J. Chem.*, 2017, **41**, 2574–2585.
70 B. van Duijneveldt, J. G. C. M. van Duijneveldt-van de Rijdt and J. H. van Lenthe, *Chem. Rev.*, 1994, **94**, 1873–1885.
71 S. F. Boys and F. Bernardi, *Mol. Phys.*, 1970, **19**, 553–566.
72 N. J. Tao and Z. Shi, *Surf. Sci.*, 1994, **301**, L217.
73 S. J. Sowerby, M. Edelwirth and W. M. Heckl, *J. Phys. Chem. B*, 1998, **102**, 5914.
74 A. Shankar, A. Jagota and J. Mittal, *J. Phys. Chem. B*, 2012, **116**, 12088.
75 W. Lv, *Chem. Phys. Lett.*, 2011, **514**, 311.

Electronic Supplementary Material (ESI) for Physical Chemistry Chemical Physics.

Theoretical Study of Gas and Solvent Phase Stability and Molecular Adsorption of Noncanonical Guanine Bases on Graphene

Nabanita Saikia[1], Shashi P. Karna[2] and Ravindra Pandey[1]

[1]Department of Physics, Michigan Technological University, Houghton, Michigan, USA

[2]Weapons and Materials Research Directorate, U.S. Army Research Laboratory, ATTN: RDRL-WM, Aberdeen Proving Ground, Aberdeen, Maryland 21005-5069, United States

AUTHOR INFORMATION

Corresponding Author

*E-mail: nsaikia@mtu.edu (N. Saikia)
pandey@mtu.edu (R. Pandey).

Telephone: +1-906-487-2086.

Table S1. Stacked and aligned configurations of $(Gua)_n$ bases: Total energy (a.u.), binding energy (E_b), and dipole moment calculated at PBE-D2 level of theory. $E_b = E_{(Gua)_n} - nE_{(Gua)}$, where E is the total energy of the system.

	$(Gua)_2$		$(Gua)_4$		$(Gua)_6$	
Gas Phase	Stacked	Aligned	Stacked	Aligned	Stacked	Aligned
Total Energy (a. u.)	-1083.9891	-1084.0079	-2168.0681	-2168.0664	-3252.0549	-3252.1027
E_b (eV)	-1.01	-1.48	-4.47	-4.29	-5.42	-6.53
Dipole Moment (Debye)	3.3	3.7	0.01	2.5	0.02	5.2
Solvent Phase						
Total Energy (a. u.)	-1084.0225	-1084.0346	-2168.1107	-2168.1173	-3252.0834	-3252.1781
E_b (eV)	-0.60	-0.72	-2.99	-3.12	-2.23	-4.73
Dipole Moment (Debye)	7.8	15.0	0.01	3.1	11.9	5.3

Table S2. $(Gua)_n$ bases with n = 2-6: The (average) intermolecular base-base bond distances (Å) calculated at the dispersion-corrected PBE-D2 and the hybrid meta-GGA M06-2X levels of theory.

System	Dispersion-corrected PBE-D2					Hybrid meta-GGA M06-2X				
	$R_{O\text{-}O}$	$R_{O\text{-}H'}$	$R_{N\text{-}H}$	$R_{N\text{-}N}$	$R_{C\text{-}C}$	$R_{O\text{-}O}$	$R_{O\text{-}H'}$	$R_{N\text{-}H}$	$R_{N\text{-}N}$	$R_{C\text{-}C}$
Gas phase										
$(Gua)_2$	3.76	2.32	4.81	3.30	4.0	3.45	3.16	1.93	4.19	4.72
$(Gua)_3$	4.11	1.94	2.61	4.23	4.57	4.11	1.96	3.42	4.62	5.01
$(Gua)_4$	3.32	3.13	1.87	4.91	4.54	4.17	2.04	2.44	5.06	5.17
$(Gua)_5$	3.30	3.15	1.83	4.93	4.54	3.46	3.07	2.30	5.09	4.78
$(Gua)_6$	3.29	3.17	1.80	4.94	4.55	3.34	3.16	1.85	5.05	4.69
Solvent phase										
$(Gua)_2$	3.40	3.25	1.86	4.99	4.54	3.54	3.16	1.99	5.07	4.67
$(Gua)_3$	4.09	1.98	2.58	4.19	4.57	4.15	1.96	3.43	4.62	5.01
$(Gua)_4$	3.24	3.24	1.84	4.92	4.50	4.18	2.04	2.44	5.06	5.17
$(Gua)_5$	3.23	3.24	1.85	4.93	4.51	3.39	3.16	1.94	5.11	4.75
$(Gua)_6$	3.23	3.25	1.80	4.93	4.50	3.35	3.17	1.87	5.08	4.71

Table S3. $(Gua)_n$ bases with n=2-6: Point group symmetry, binding energy (E_b), binding energy per base (E_b/n), and (average) intermolecular R_{O-H} distance calculated at the wB97XD and M05-2X levels of theory. $E_b = E_{(Gua)_n} - nE_{Gua}$, where n is the number of Gua bases and E is total energy of the system.

	wB97XD				Hybrid meta-GGA M05-2X			
	Symmetry	E_b (eV)	E_b/n (eV)	R_{O-H} (Å)	Symmetry	E_b (eV)	E_b/n (eV)	R_{O-H} (Å)
Gas phase								
$(Gua)_2$	C_2	-1.39	-0.70	1.74	C_1	-1.36	-0.68	1.78
$(Gua)_3$	C_3	-2.85	-0.95	1.86	C_1	-2.75	-0.92	1.85
$(Gua)_4$	S_4	-4.01	-1.00	1.73	C_{4h}	-3.87	-0.97	1.87
$(Gua)_5$	C_1	-5.03	-1.01	1.78	C_1	-4.72	-0.94	1.90
$(Gua)_6$	C_2	-6.04	-1.01	1.81	C_1	-5.62	-0.94	1.91
Solvent phase								
$(Gua)_2$	C_1	-0.64	-0.32	1.86	C_2	-0.56	-0.28	1.78
$(Gua)_3$	C_3	-1.64	-0.55	1.83	C_3	-1.49	-0.50	1.85
$(Gua)_4$	C_2	-2.63	-0.66	1.77	S_4	-2.33	-0.58	1.91
$(Gua)_5$	C_1	-3.36	-0.67	1.81	C_1	-2.90	-0.58	1.90
$(Gua)_6$	C_1	-4.33	-0.72	1.80	C_1	-3.50	-0.58	1.91

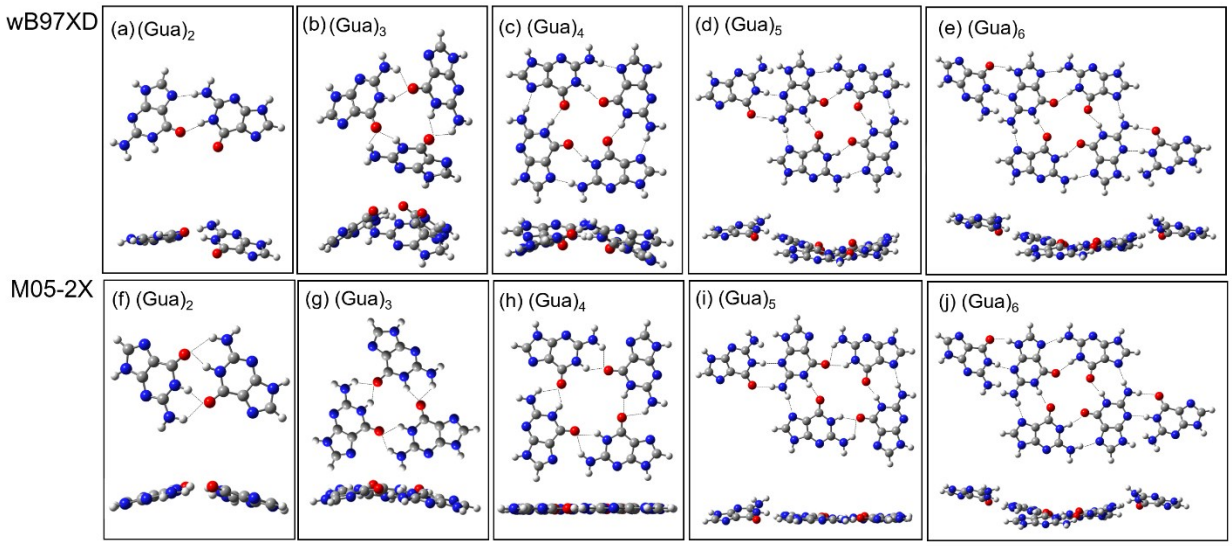

FIG. S1. Solvent-phase equilibrium configurations of $(Gua)_n$ bases obtained at the (a-e) wB97XD, and (f-j) M05-2X levels of theory.

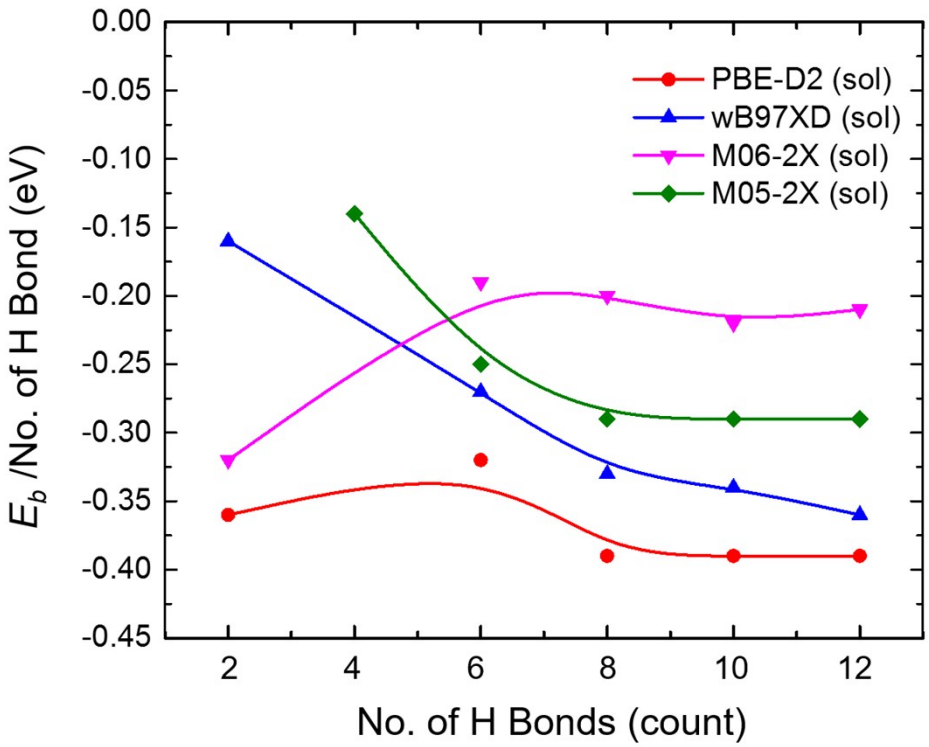

FIG. S2. The relative stability of $(Gua)_n$ bases obtained at the PBE-D2 and M06-2X levels of theory in solvent phase.

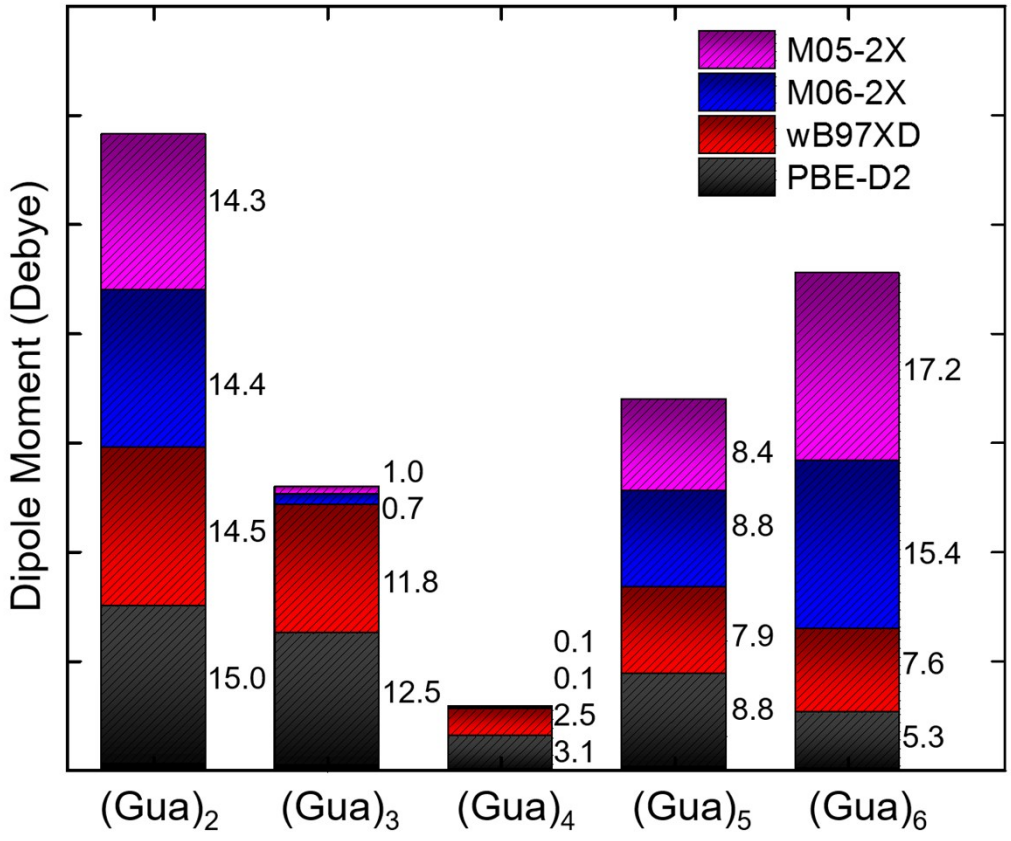

FIG. S3. Calculated dipole moments for $(Gua)_n$ bases obtained at the PBE-D2, wB97XD, M06-2X and M05-2X levels of theory in solvent phase.

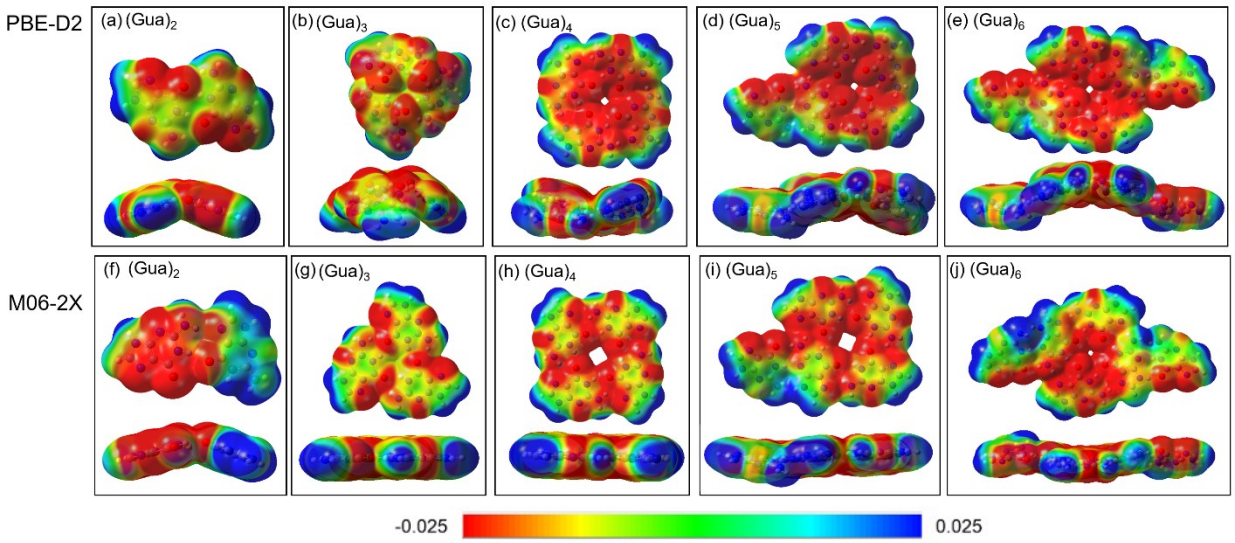

FIG. S4. ESP isosurfaces of $(Gua)_n$ complexes in gas phase: (a)-(e) PBE-D2 and (f)-(j) M06-2X levels of theory.

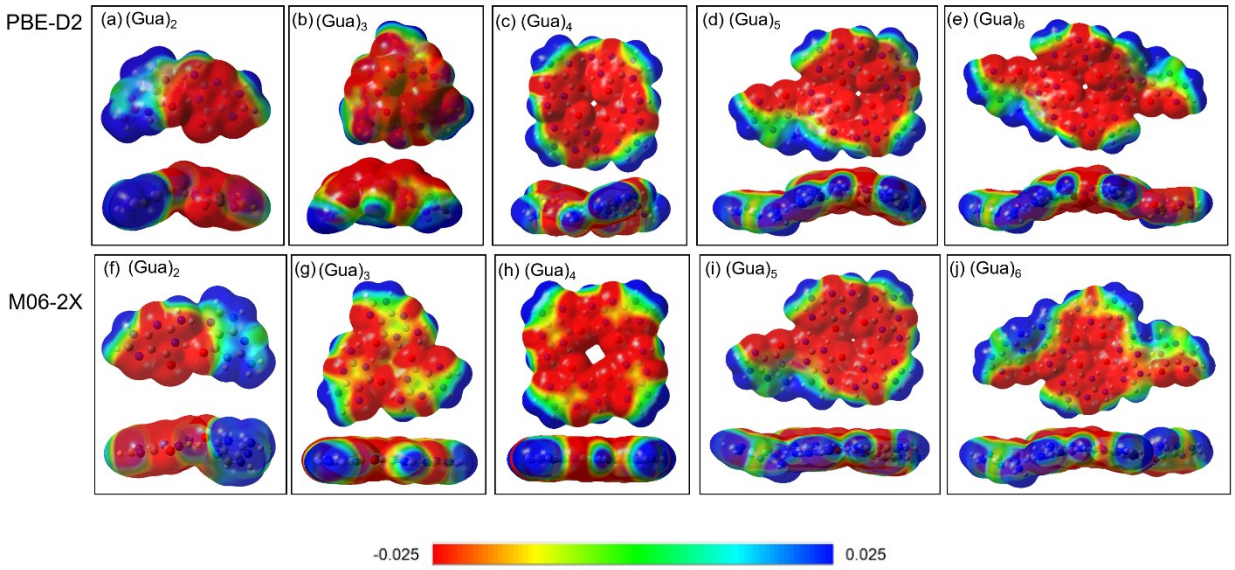

FIG. S5. ESP isosurfaces of $(Gua)_n$ complexes in solvent: (a)-(e) PBE-D2 and (f)-(j) M06-2X levels of theory.

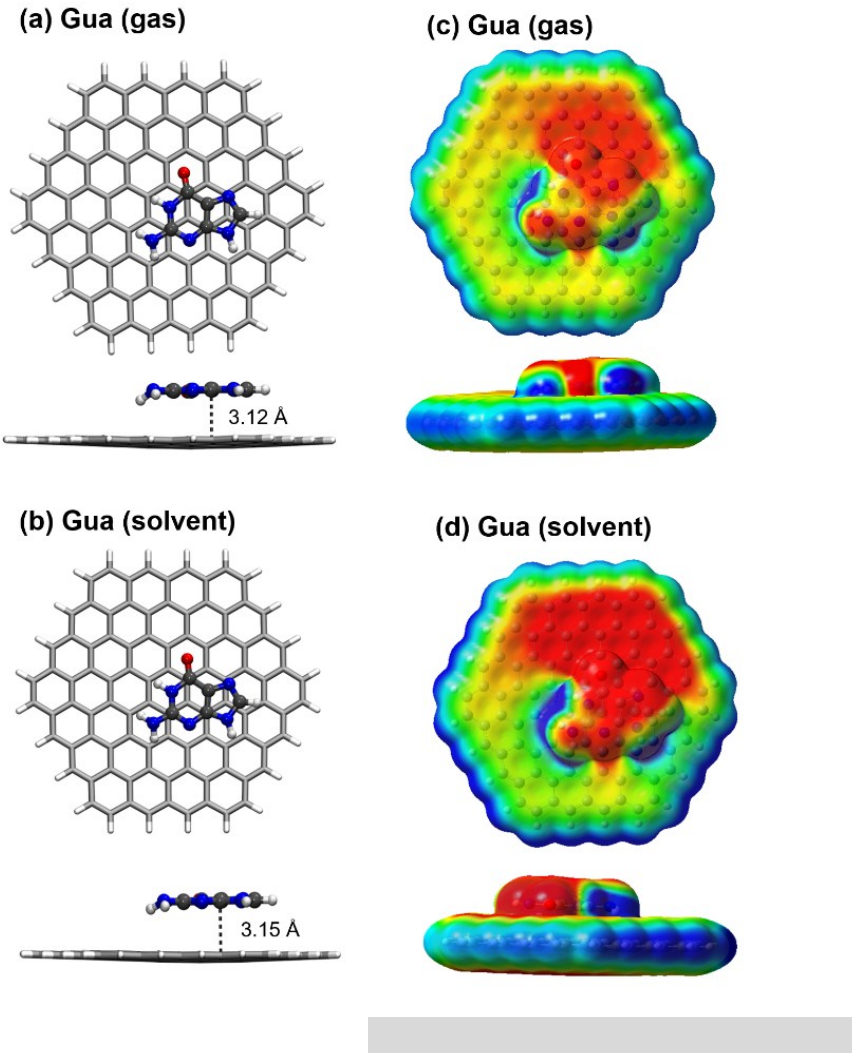

FIG. S6. Calculated equilibrium configurations and ESP isosurfaces of (Gua)/Graphene in gas and solvent phases.

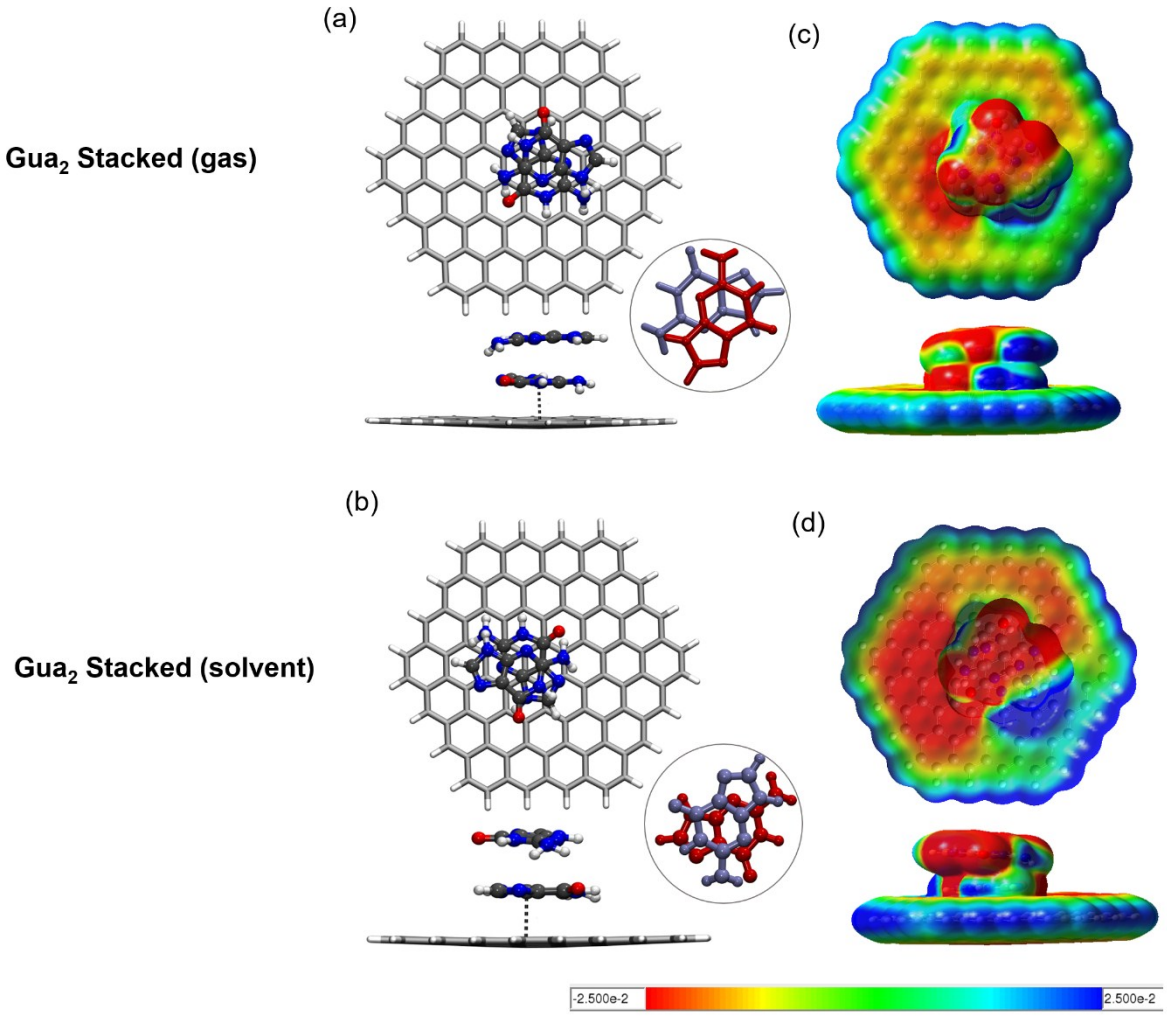

FIG. S7. Calculated equilibrium configurations and ESP isosurfaces of $(Gua)_2$/Graphene in the stacked base configuration in gas and solvent phases.

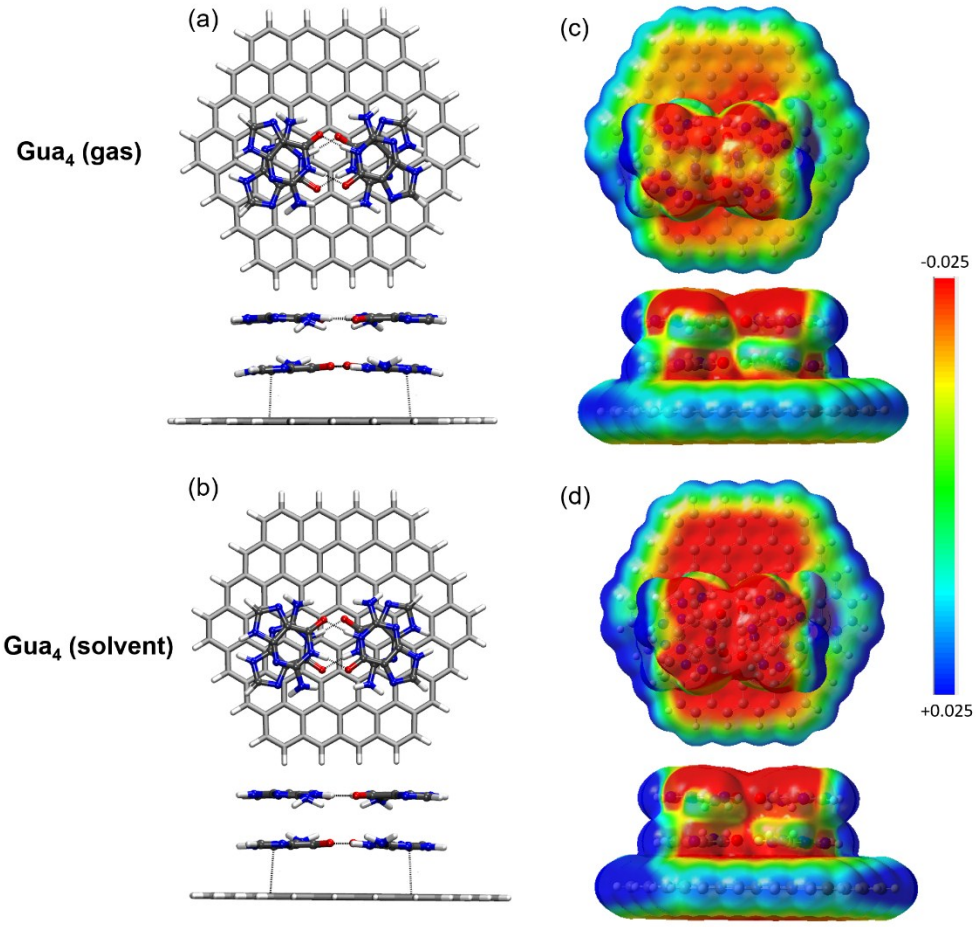

FIG. S8. Calculated equilibrium configurations and ESP isosurfaces of $(Gua)_4$/Graphene in the stacked base configuration in gas and solvent phases.

Gua/Graphene complex: Gas-phase interaction of a single Gua base with graphene was previously investigated in a periodic supercell model in the framework of vdW-corrected DFT.[S1] The PBE-D2 calculations found the base-substrate distance to be 3.26 Å with the interaction energy of -1.18 eV for the Gua/graphene complex. Employing the same level of theory, our cluster model finds the base-substrate distance to be 3.12 Å and the interaction energy to be -1.02 eV for the Gua/graphene complex (Table S4), thus showing qualitative agreement between the results obtained from the cluster and periodic supercell models. Note that a small difference between the base-substrate distance and the interaction energy is likely due to different basis sets employed in these calculations.

Table S4. Gua/Graphene complex: Interaction energies (E_{int}, eV), interplanar base-substrate distance (Å), dipole moment (Debye) calculated using the PBE-D2 level of theory.

	System	E_{int} **(eV)**	**Distance (Å)**	**Dipole moment (Debye)**
Cluster Model (This work)	Gas phase	-1.02	3.12	2.88
	Solvent phase	-0.82	3.15	7.65
Ref. S1 (PBE + vdW) (Periodic Supercell model)	Gas phase	-1.18	3.26	-

[S1] J.-H. Lee, Y.-K. Choi, H.-J. Kim, R. H. Scheicher, J.-H. Cho, J. Phys. Chem. C 117, 13435 (2013).